Available online at www.sciencedirect.com

SciVerse ScienceDirect

Geochimica et Cosmochimica Acta 76 (2012) 161–174

Geochimica et Cosmochimica Acta

www.elsevier.com/locate/gca

Magnesium isotope fractionation during hydrous magnesium carbonate precipitation with and without cyanobacteria

Vasileios Mavromatis [a,*], Christopher R. Pearce [a,1], Liudmila S. Shirokova [a,b], Irina A. Bundeleva [a], Oleg S. Pokrovsky [a], Pascale Benezeth [a], Eric H. Oelkers [a]

[a] *Geosciences Environment Toulouse (GET), CNRS, UMR 5563, Observatoire Midi-Pyrénées, 14 Avenue Edouard Belin, 31400 Toulouse, France*

[b] *Institute of Ecological Problems of the North, 23 Nab. Sev. Dviny, Russian Academy of Science, Arkhangelsk, Russia*

Received 27 April 2011; accepted in revised form 30 September 2011; available online 17 October 2011

Abstract

The hydrous magnesium carbonates, nesquehonite ($MgCO_3 \cdot 3H_2O$) and dypingite ($Mg_5(CO_3)_4(OH)_2 \cdot 5(H_2O)$), were precipitated at 25 °C in batch reactors from aqueous solutions containing 0.05 M $NaHCO_3$ and 0.025 M $MgCl_2$ and in the presence and absence of live photosynthesizing *Gloeocapsa* sp. cyanobacteria. Experiments were performed under a variety of conditions; the reactive fluid/bacteria/mineral suspensions were continuously stirred, and/or air bubbled in most experiments, and exposed to various durations of light exposure. Bulk precipitation rates are not affected by the presence of bacteria although the solution pH and the degree of fluid supersaturation with respect to magnesium carbonates increase due to photosynthesis. Lighter Mg isotopes are preferentially incorporated into the precipitated solids in all experiments. Mg isotope fractionation between the mineral and fluid in the abiotic experiments is identical, within uncertainty, to that measured in cyanobacteria-bearing experiments; measured $\delta^{26}Mg$ ranges from −1.54‰ to −1.16‰ in all experiments. Mg isotope fractionation is also found to be independent of reactive solution pH and Mg, CO_3^{2-}, and biomass concentrations. Taken together, these observations suggest that *Gloeocapsa* sp. cyanobacterium does not appreciably affect magnesium isotope fractionation between aqueous fluid and hydrous magnesium carbonates.

1. INTRODUCTION

Biomineralization is the most important carbonate mineral formation mechanism in the hydrosphere (Lowenstam and Weiner, 1989; Chafetz and Buczynski, 1992; Ferris et al., 1997; Douglas and Beveridge, 1998; Dove, 2010). Cyanobacteria induced mineralization occurred in both ancient and modern environments (Brady et al., 2009; Planavsky et al., 2009; Raven and Giordano, 2009); cyanobacteria-dominated carbonate formation occurred in oceans, lakes, springs, and soils during the Precambrian (Riding, 2000), whilst modern cyanobacteria-dominated carbonate formation occurs in highly alkaline aquatic environments (Thompson and Ferris, 1990; Braithwaite and Zedef, 1994; Dupraz et al., 2009; Power et al., 2009). Locations where modern cyanobacteria-dominated magnesium carbonate formation occurs include Lake Salda in Turkey, which is fed by ultramafic rock weathering products (e.g. Braithwaite and Zedef, 1994; Shirokova et al., 2011), and alkaline lakes such as those in British Columbia (Power et al., 2007, 2009).

The chemical and isotopic composition of microbially induced minerals is routinely used to reconstruct past environmental conditions (Altermann et al., 2006), with particular emphasis on carbon and oxygen fractionation in carbonates (e.g. Pentecost and Spiro, 1990; Power et al., 2007). Until recently, little attention has been paid

* Corresponding author. Tel.: +33 5 61 33 25 66; fax: +33 5 61 33 25 60.

E-mail address: mavromat@lmtg.obs-mip.fr (V. Mavromatis).

[1] Present address: Department of Earth and Environmental Sciences, The Open University, Walton Hall, Milton Keynes MK7 6AA, UK.

0016-7037/$ - see front matter © 2011 Elsevier Ltd. All rights reserved.
doi:10.1016/j.gca.2011.10.019

to the possibility of isotopic fractionation of the major divalent cations (i.e. Ca, Mg, and Sr) within carbonate minerals owing to the more complex analytical procedures required to quantify these effects (Chang et al., 2003; Young and Galy, 2004). The importance of Mg in biogeochemical cycles, and the ~8% mass difference between ^{24}Mg and ^{26}Mg suggest that Mg isotopes are potentially useful for resolving natural carbonate precipitation mechanisms. The potential for magnesium isotope fractionation in carbonate minerals has been recently documented for Mg-bearing carbonates (Chang et al., 2004; Buhl et al., 2007; Hippler et al., 2009). The degree to which microbes may influence this fractionation has yet to be investigated quantitatively. The goal of this study is to overcome this knowledge gap by directly measuring the magnitude of Mg isotope fractionation during the abiotic and cyanobacteria induced precipitation of hydrous Mg-carbonates. Results of these experiments are used to (i) calibrate Mg isotope fractionation between aqueous solutions and biotically and abiotically formed hydrous magnesium carbonates at Earth surface conditions, and (ii) assess of the possible role of cyanobacteria on Mg isotope fractionation during bio-induced carbonate mineralization.

2. MATERIALS AND METHODS

2.1. Culture and characterization of cyanobacteria

An axenic culture of mesophilic *Gloeocapsa* sp. f-6gl cyanobacteria isolated from a spring in Kamchatka, Russia and described earlier (Pokrovsky et al., 2008) was used in this study. The bacterium was grown in synthetic, low-phosphate (10% of normal content) cyanobacteria BG-11 Freshwater Solution for 3 weeks until the stationary growth phase was attained (c.f. Martinez et al., 2008). Cyanobacterium *Gloeocapsa* sp. typically consists of a small number of individual spherical colonies, each containing 3–10 cells enclosed within larger mucilage masses. The concentration of the bacterial cell suspensions was quantified via optical density (OD) using a spectrophotometer at a wavelength of 750 nm. This wavelength was selected after spectra recording in the 300–800 nm region of both (1) mineral-free, live *Gloeocapsa* sp. cyanobacteria bearing suspensions, and (2) dypingite bearing, cell-free suspensions. The cell-free suspensions exhibit no adsorption in the 650–800 nm region whereas the cyanobacterial cell-bearing suspensions exhibit a distinct peak at 700–750 nm. The overall light absorbance of mineral-bearing suspensions is a factor of 10 lower than that of the mineral-free, live biomass bearing suspensions, when normalized to dry or wet weight. As a result, the maximum uncertainty in biomass concentrations obtained via optical absorbance at 750 nm induced by the presence of minerals is no more than 10%, which is within the experimental reproducibility. The OD – biomass calibration curve was linear for up to 1.3 absorbance units and the ratio between humid and freeze-dried weight of *Gloeocapsa* sp. was 10.0 ± 2.0. Although the experiments were conducted under fully sterile conditions, possible reactor contamination by other cyanobacteria species and culturable aerobic heterotrophic bacteria was assessed weekly by a detailed optical microscopic examination of the bacterial culture following its growth on agar plates containing BG-11 or nutrient agar. No detectable contamination was observed even during long-term experiments.

2.2. Precipitation experiments

Precipitation experiments were performed in 1000 ml sterile borosilicate glass reactors containing either the low-phosphate BG-11 growth medium or the cell supernatant, into which 25–30 mM $MgCl_2$ and ~50 mM $NaHCO_3$ were added. These conditions were found to be both (1) suitable for Mg carbonate precipitation and (2) correspond closely to conditions found in natural settings where hydromagnesite precipitation has been reported (Braithwaite and Zedef, 1994; Power et al., 2007; Shirokova et al., 2011). Experiments with lower concentrations of $MgCl_2$ and $NaHCO_3$ failed to produce sufficient precipitation for analysis, whereas higher concentrations led to rapid and uncontrolled hydrous Mg carbonate precipitation. The low-phosphate BG-11 growth medium used for these experiments had the composition of the traditional BG-11 growth medium other than its P content; the low phosphate growth medium contained only 50 μM P, which is 10% that of the traditional medium (c.f. Martinez et al., 2008). The bacteria used in the experiments were pre-cultured in low phosphate BG-11 media before being placed in the reactors. The bacteria continued to grow while mineral precipitation occurred; biomass typically increased by a factor of 10 during the first 2–4 weeks then increased less rapidly for the rest of the mineral precipitation experiments. Details of all experiments performed in this study are given in Table 1.

All experiments were performed at 25 ± 2 °C. Some were conducted in reactors that were continuously stirred and bubbled with air. These conditions were chosen to reduce heterogeneities in the bulk fluid composition and the cell/precipitate distribution in the reactors. In addition, air bubbling fixed the CO_2 content in the reactor fluids. Since the homogeneous nucleation of carbonates can be influenced by stirring (Pokrovsky and Savenko, 1995a; Pokrovsky, 1998), several experiments were also conducted by shaking the reactors rather than either bubbling and/or stirring. Such experiments provide insight into the possible role of fluid hydrodynamics and Mg diffusion on precipitation rates, precipitate identity, and Mg-isotopic fractionation. Several additional experiments were performed without shaking and air bubbling in an attempt to reproduce natural conditions such as those associated with carbonate precipitation in shallow biomats. Each experiment is described in detail below.

All biotic experiments were initiated by adding a known quantity of previously grown *Gloeocapsa* sp. cyanobacteria to the reactors. Experiments Bio-A and Bio-B were performed in reactors that were continuously stirred with a magnetic stirring bar at 150 rpm and bubbled with sterile humid air with an average flow rate of 1.5 ± 0.3 L/min. Experiments Bio-C and Bio-F were performed in reactors that were neither shaken, nor stirred, nor air bubbled. Experiment Bio-D was shaken continuous using a Fisher PingPong 400 shaker at a rate of 120 movements/min,

Table 1
Experimental conditions of all experiments performed in this study. All initial fluids contained 0.025–0.032 M $MgCl_2$ and 0.05 M $NaHCO_3$ except Abio-B which contained 0.05 M $MgCl_2$ and 0.01 M $NaHCO_3$. All abiotic experiments were conducted in the presence of 0.01 M NaN_3 to avoid possible microbial contamination. All experiments were performed under continuous light unless indicated. The Mg concentration range indicates total Mg concentration range measured at various during each experiment.

Experiment	Medium	Duration (days)	pH range	Mg concentration range ($\times 10^{-3}$ mol L^{-1})	DOC (mg/L)	Conditions
Bio-A	Low P BG-11	30	8.2–10.4	25–4	50	Stirring, bubbling
Bio-B	Low P BG-11	27	8.3–10.0	26–13	60	Stirring, bubbling
Bio-C	Low P BG-11	42	8.3–10.0	31–7	9.5	No stirring, no bubbling
Bio-D	Low P BG-11	42	8.3–10.2	28–7	34	Shaking, no bubbling
Bio-E	BG-11	45	8.6–9.4	29–17	30	Stirring, no bubbling
Bio-F	Low P BG-11	45	8.5–9.4	30–18	27	No stirring, no bubbling
Bio-G	Low P BG-11	143	8.3–10.0	28–8	5	No stirring, no bubbling Day/night cycle
Bio-I	Low P BG-11	143	8.3–9.4	29–15	2	Shaking, no bubbling, darkness
Abio-A	Sterile supernatant	25	8.1–9.3	29–12	60	Stirring, bubbling
Abio-B	Sterile supernatant	67	8.7–9.4	47–16	61	Stirring, bubbling
Abio-C	Sterile supernatant	67	8.0–9.4	32–21	20	Stirring, no bubbling
Abio-D1	BG-11[a]	73	8.6–9.5	32–14	30	Stirring, bubbling
Abio-D2	Low P BG-11	73	8.7–9.3	32–13	31	Stirring, bubbling
Abio-E	Sterile supernatant	20	8.0–9.3	32–19	50	Stirring, bubbling
Min-free	Low P BG-11	44	8.2–10.65	0.003–0.006		Precipitation free

[a] BG-11 with normal PO_4 content.

whereas experiment Bio-E was continuous stirred. Both experiment Bio-D and Bio-E were performed in the absence of bubbling. Each of these experiments (Bio-A to Bio-F) was performed under continuous fluorescent light of 30 μmol photon m^{-2} s^{-1}. In addition, experiment Bio-G was run under a normal day/night cycle without stirring and bubbling and experiment Bio-I was shaken and run in complete darkness without bubbling. Furthermore, experiments Bio-G and Bio-I run for 143 days (i) to observe the end of the stationary growth phase and beginning of the cell death phase and (ii) to assess possible long-term mineral transformations. As such these two experiments more closely approximated natural conditions where mineral transformation could occur.

Abiotic experiments Abio-A, Abio-B, Abio-C, and Abio-E were performed in the presence of a sterile supernatant of the *Gloeocapsa* sp. cyanobacteria to which were added $MgCl_2$ and $NaHCO_3$ in similar concentrations to those of the biotic experiments and 50 ± 10 mg/L of dissolved organic carbon (DOC) in the form of cell exometabolites. The supernatant solution for the abiotic experiments was generated via centrifugation and filtration through a 0.22 μm filter of a *Gloeocapsa* sp. culture collected at the stationary stage. The term cell exometabolites refers to dissolved (<0.22 μm) organic substances of undefined structure and chemical composition, largely dominated by exopolysaccharides. Note that phytoplankton-originated exopolymeric substances represent the major pool of autochthonous organic matter in natural waters, including the lakes where hydrous Mg carbonate precipitation occurs. The amount of Mg initially present in the supernatant was always less than 5% of that added in the form of $MgCl_2$. The concentration of DOC used in these experiments is similar to that measured in the experiments containing the live *Gloeocapsa* sp. Abiotic control experiments Abio-D1 and Abio-D2 were performed in sterile low-phosphate and traditional BG-11 culture media, respectively. Experiments Abio-A, Abio-B, Abio-D1, Abio-D2, and Abio-E were bubbled with sterile humid air at similar flow rates as that of experiments Bio-A and Bio-B. All abiotic experiments were performed in the presence of 0.01 M NaN_3 to prevent possible microbial contamination.

One additional experiment, Min-free, was run to assess Mg consumption and isotopic fractionation by *Gloeocapsa* sp. in the absence of carbonate precipitation. This experiment was performed in BG-11 medium originally containing 0.30 mM $MgSO_4$ and 4 mM $NaHCO_3$. The fluid phase and biomass in this experiment were sampled after 11 and 44 days of growth.

2.3. Sampling and analyses

30–50 ml aliquots of homogeneous suspension containing the fluid, precipitated minerals, and cells if present were sampled periodically from the reactors in a sterile laminar hood box during each experiment (see Table ESM-1). The optical density and pH were measured in suspension subsamples, whilst the fluid supernatants were filtered using MilliPore 0.22 μm cellulose acetate filters, then used for alkalinity, DOC, and Mg concentration measurements. Alkalinity was determined following a standard HCl titration procedure using an automatic Schott TitroLine alpha $TA10^{plus}$ titrator with an uncertainty of ±2% and a detection limit of 5×10^{-5} M. DOC was analyzed using a Shimadzu TOC-6000 Carbon Total Analyzer with an uncertainty of 3% and a detection limit of 0.1 mg/L. Magnesium concentrations were measured by flame atomic absorption spectroscopy using a Perkin Elmer AAnalyst 400 with an uncertainty of ±2% and a detection limit of 2×10^{-7} M. pH was measured using a Mettler Toledo

combined electrode, with a precision of ±0.001. The uncertainty of biomass concentration determination via optical density is estimated at ±10%.

Organic matter was removed from the surfaces of a subset of the recovered minerals prior to their surface characterization by treating them with 10% H_2O_2 for 2–3 days at the same pH as the experimental fluids. The residual solid phases were then thoroughly rinsed in de-ionized water and freeze dried at −55 °C. The resulting mineral phases were characterized by scanning electron microscopy (SEM) using a Jeol JSM840a, and by X-ray diffraction using an INEL CPS 120 $Co_{K\alpha}$, with a scan speed of 0.02° s^{-1}. Mineral-free bacterial cells and cell biomass with precipitated carbonates were also observed using Transmission Electron Microscopy (TEM) with a JEOL JEM 12000 EX and a JEOL JEM 2100F equipped with a field emission gum (FEG) and PGT EDX detector at 80 kV. TEM samples were prepared by first rinsing cell suspension with sterile nutrient solution and MilliQ water then centrifuging them for about 2 min at 10,000 rpm. TEM analyses were then performed on grids coated with a carbon film that was submerged in the prepared bacterial suspension for 10 s then dried.

2.4. Magnesium isotope analyses

Mg isotope compositions of both filtered fluids and solid phases were measured. The Mg compositions of the solids were measured before any pre-treatment; as such resulting Mg compositions reflect contributions of the precipitated mineral and some organic material, including cells of cyanobacteria and chlorophyll-*a*. The fraction of Mg incorporated in the organic material during cell growth is estimated to be less than ~0.1% of the total amount of Mg precipitated from the reactive solutions during the experiments (see Section 4.2 for details). Because precipitation was performed under controlled conditions, the potential for isobaric interferences from double charged ions (e.g. $^{48}Ca^{2+}$, $^{48}Ti^{2+}$, $^{50}Ti^{2+}$, $^{50}V^{2+}$, $^{50}Cr^{2+}$, and $^{52}Cr^{2+}$) was minimal. Galy et al. (2001), however, demonstrated that the presence of Na^+ and other species within the sample matrix could also result in mass bias effects. Consequently all samples were chemically purified prior to Mg isotope analysis via cation exchange chromatography. Filtered acidified fluids were evaporated to dryness and re-diluted in 1 M HNO_3, while the freeze-dried solid samples and mineral-free organic samples obtained from experiment Min-free were digested in 16 M HNO_3, before being evaporated and re-dissolved in 1 M HNO_3. Mg separation was achieved using the protocol of Teng et al. (2007), with the AG 50W-X12 exchange resin held in a 10 ml Bio-Rad poly-prep column. Complete recovery of Mg from the columns, which is essential to avoid isotopic fractionation (Chang et al., 2003; Teng et al., 2007) was confirmed by replicate passes of samples with different matrices through the resin column (Pearce et al., 2009). A single pass was generally sufficient to reduce the cation/Mg ratio in the sample to <0.05, thereby avoiding potential interferences during mass spectrometry analysis (Galy et al., 2001).

Magnesium isotopic ratios were measured using a Thermo-Finnigan 'Neptune' Multi Collector Inductively Coupled Plasma Mass Spectrometer (MC–ICP-MS) at both the GET (Toulouse, France) and at The Open University (Milton Keynes, UK). All solutions were prepared in 0.32 M HNO_3 and were introduced into the Ar plasma using a standard spray chamber. Instrumental mass fractionation effects were corrected via sample-standard bracketing, and all results are presented in delta notation with respect to the DSM3 international reference material (Galy et al., 2001; Goldstein et al., 2003):

$$\delta^x Mg = \left(\frac{\left(\frac{^xMg}{^{24}Mg}\right)_{sample}}{\left(\frac{^xMg}{^{24}Mg}\right)_{DSM3}} - 1 \right) \times 1000 \quad (1)$$

where x refers to the Mg mass of interest. Compatibility of results between the two MC–ICP-MS used in this study was confirmed by replicate analyses of three international Mg reference standards (DSM3, CAM-1, and OUMg), and by duplicate analyses of the carbonate standard J-Do 1. The $\delta^{26}Mg$ reproducibility of these standards was typically <0.07‰.

The isotopic offset between the Mg in the fluid and that incorporated into the solid phase can be defined as:

$$\Delta^{26}Mg_{solid-liquid} \equiv \delta^{26}Mg_{solid} - \delta^{26}Mg_{liquid} \quad (2)$$

This value was determined for all samples where both the fluid and solid phases were collected in the present study.

The evolution of the Mg isotopic composition of the solid phase ($\delta^{26}Mg_{solid}$) precipitating in a closed system experiment can be calculated from mass balance constraints using (Criss, 1999):

$$\delta^{26}Mg_{solid} = \delta^{26}Mg_{initial} + A(\Delta^{26}Mg_{solid-liquid} - 1) \times 10^3 \quad (3)$$

where A stands for the percent of Mg precipitated from the liquid phase, and $\delta^{26}Mg_{initial}$ refers to the isotopic composition of the initial fluid phase.

3. RESULTS

The measured chemical composition of the reactive fluids (e.g. the fluid phase in the reactor during the experiments) and the mineralogy of precipitated solid phases in all samples are listed in the Electronic Supplementary Material Table ESM-1 (file ESM.pdf) and are described in detail below.

3.1. Mineralogy of the precipitated phases

Examples of X-ray diffraction patterns of the solid phases precipitated during the experiments are shown in Fig. 1. X-ray diffraction results demonstrate the precipitation of nesquehonite ($MgCO_3$ $3H_2O$) and dypingite ($Mg_5(CO_3)_4(OH)_2$ $5H_2O$) at distinct times during the experiments. Nesquehonite precipitation is limited to the first hours of experiments Bio-A and Abio-A. After ~100 h of reaction time, dypingite was the only mineral phase present in these experiments. Experiments Bio-C, Bio-D, and Abio-D2 exhibit dypingite formation whereas experiments Bio-F,

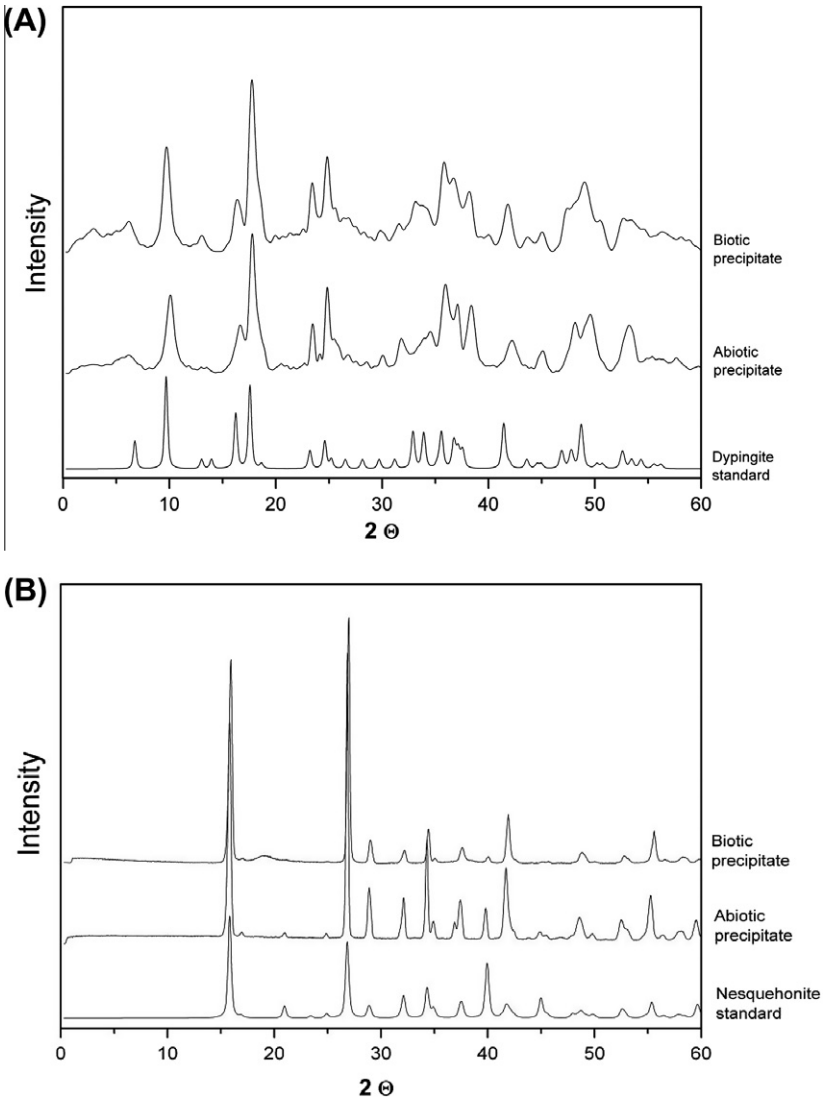

Fig. 1. X-ray diffraction patterns of the solids recovered from (A) experiments Bio-A after 30 days and Abio-A after 27 days, and (B) experiments Bio-B after 23 days and Abio-C after 15 days compared to reference X-ray diffraction patterns of dypingite and nesquehonite, respectively.

Bio-G, Bio-I, Abio-B, Abio-C, Abio-D1, and Abio-E exhibit nesquehonite formation. Co-existence of both mineral phases was observed only in the final solid sample collected from experiment Bio-E. In general, all the collected nesquehonite XRD patterns exhibited close agreement with its corresponding reference pattern (see Fig. 1B), whilst the collected XRD patterns of collected dypingite exhibit some minor difference compared to its corresponding reference pattern (see Fig. 1A). No clear connection between the mineralogy of the precipitated phase and the experimental/physical conditions of the experiment is evident. Scanning electron microscopy images reveal that nesquehonite exhibits a needle-like habit with needles ranging from 5 to 15 μm in length (see Fig. 2A), whilst the dypingite is present as 2–8 μm diameter rosette-like aggregates (see Fig. 2B and C). Transmission electron microscopy demonstrated the presence of nanometer size mineral precipitates in the vicinity of cell surfaces in solutions supersaturated with respect to hydrous Mg carbonates (see Fig. 3A and B) suggesting a direct link between the bacteria and some precipitates. The chemical analysis of these precipitates taken at the position of the cross in Fig. 3B, indicated that Mg, C, and O are the main elements and the concentration of P, S, and Cl are negligible. Such cell associated precipitates were absent in control media (see Fig. 3C).

3.2. Chemical composition of the fluid phase

The temporal evolution of Mg concentration and pH in all experiments as well as alkalinity and biomass concentration during representative experiments are illustrated in Fig. 4. The Mg concentration and alkalinity of the reactive fluids tend to decrease and the pH tends to increase with time during all biotic experiments. Some significant

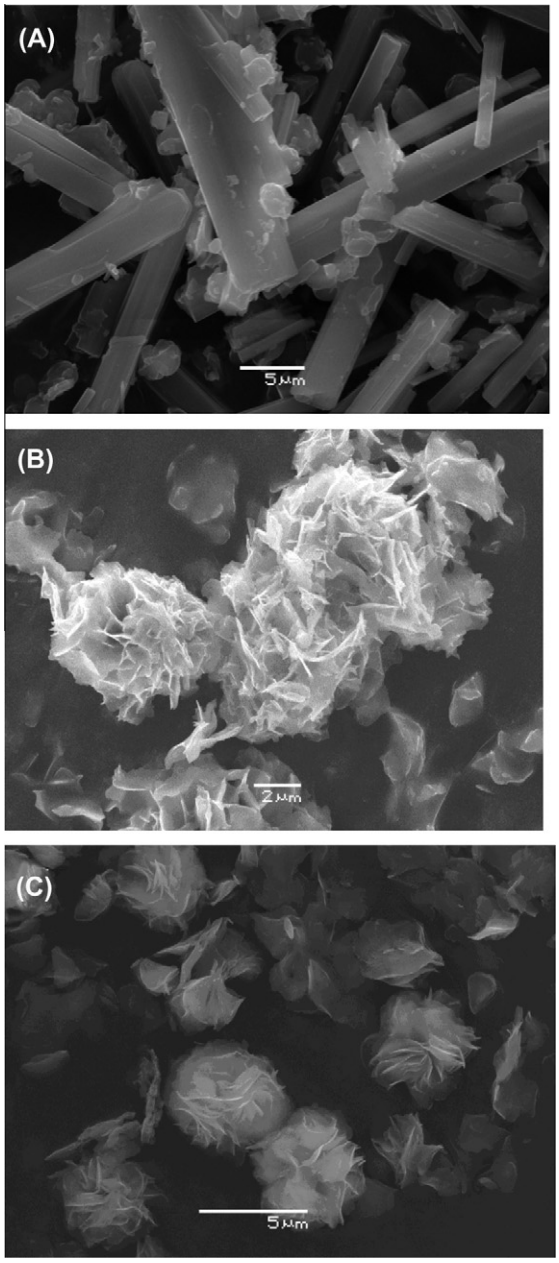

Fig. 2. SEM images of hydrous magnesium carbonate phases precipitated during this study: Nesquehonite needles collected from (A) experiment Bio-A after ~1 h, (B); dypingite rosettes collected from experiment Bio-A after 30 days, and (C) Abio-A after 27 days.

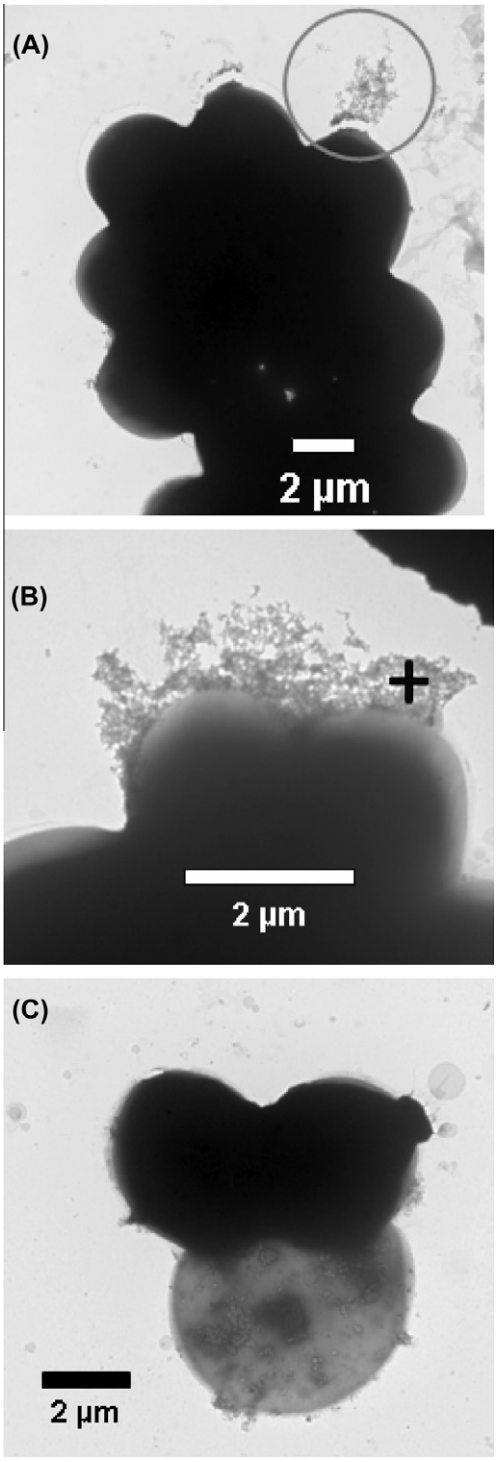

Fig. 3. TEM images of active *Gloeocapsa* sp. cyanobacteria and associated precipitates collected after 14 days from $MgCl_2$–$NaHCO_3$ enriched BG-11 medium (A and B) and from BG-11 medium undersaturated with respect to Mg hydrous carbonates (C). The solid precipitates are encircled in A. Chemical composition of these precipitates (taken at the position of cross in Fig. 3B) yielded Mg, C, and O as main elements with insignificant amount of P, S, and Cl.

differences, however, are evident among the biotic experiments. For example, an initial latent stage lasting ~4 days is observed in experiments Bio-A, Bio-B, Bio-E, and Bio-F, during which the reactive fluid exhibits a slight increase in Mg concentration and alkalinity. This latent stage is followed by a rapid decrease in reactive fluid Mg concentration and alkalinity during the next 10–15 days, before attainment of a quasi-stationary state. Experiments Bio-C, Bio-D, Bio-G, and Bio-I exhibit similar temporal Mg concentration and pH variations, although a pH drop accompanied by an increase in the Mg concentration and alkalinity are observed after 40–60 days. For all of these

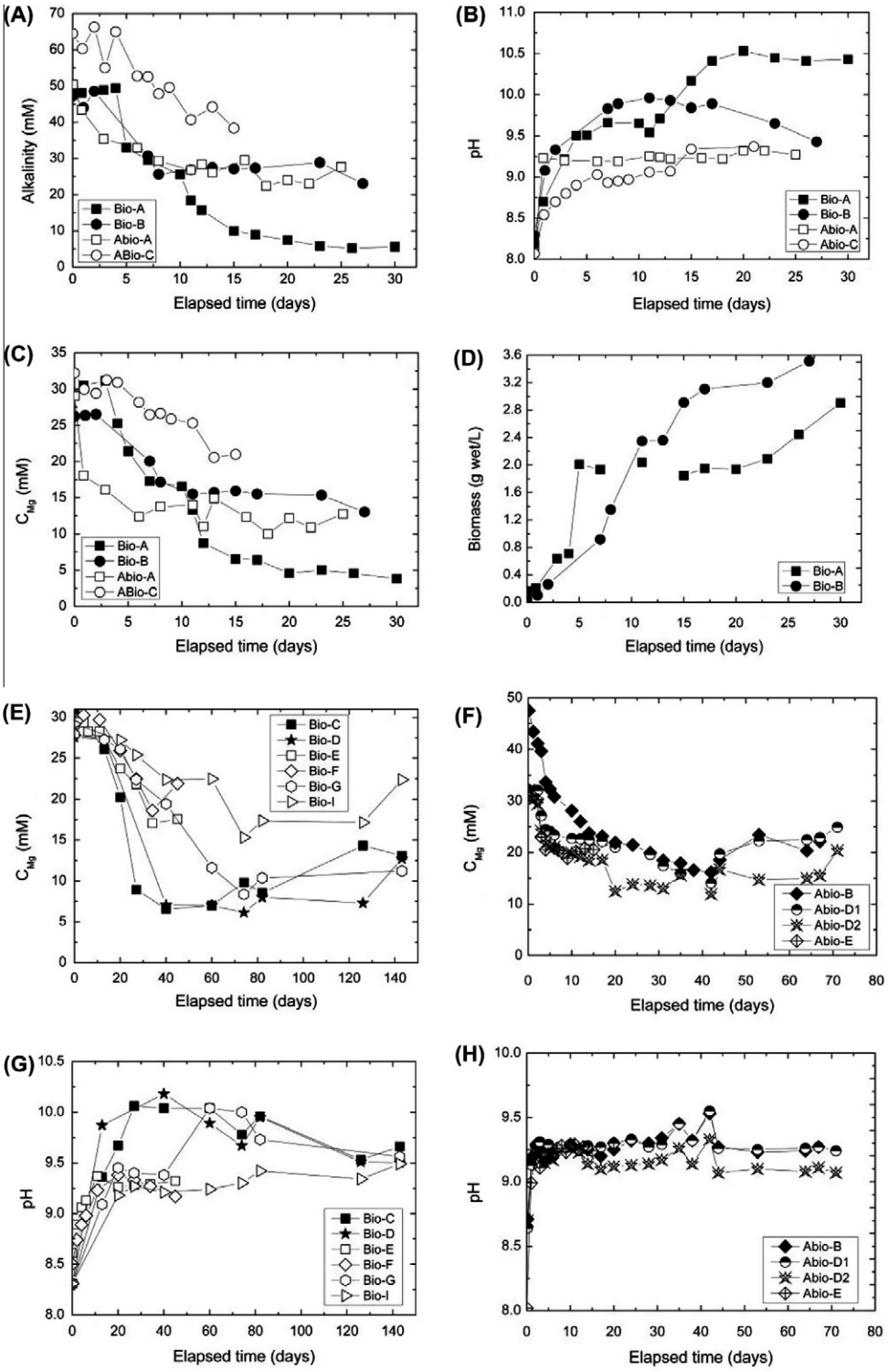

Fig. 4. Reactive fluid evolution during the experiments performed in this study. Temporal evolution of (A) alkalinity, (B) pH, (C) Mg concentration (C_{Mg}), and (D) biomass concentration during experiments Bio-A, Bio-B, Abio-A, and Abio-C. Temporal evolution of (E) Mg concentration and (G) pH during experiments Bio-C, Bio-D, Bio-E, Bio-F, Bio-G, and Bio-I. Temporal evolution of (F) Mg concentration and (H) pH during experiments Abio-B, Abio-D1, Abio-D2, and Abio-E. The symbol size approximates the uncertainty of the analyses.

biotic experiments other than Bio-I, this final pH drop is concurrent with a decrease of fluid optical density suggesting that this observation stems from cyanobacterial death. A decrease in photosynthetic activity due to decreasing cyanobacterial activity can result in decreasing pH which favors Mg-carbonate dissolution.

In the abiotic experiments, the reactive fluid Mg concentration and alkalinity decreased during the first 10 ± 5 days, becoming almost constant thereafter, suggesting the attainment of near-equilibrium conditions. During the same period, the reactive fluid pH increased to 9.2–9.3 and then remained approximately constant until the end of each experiment (see Fig. 4 and Table ESM-1).

The speciation and saturation state of the reactive fluids with respect to potentially precipitating mineral phases for all experiments was calculated using PHREEQC together with its MINTEQA2 database (Parkhurst and Appelo, 1999) after adding to it thermodynamic properties for nesquehonite and hydromagnesite reported by Cheng and Li (2010a,b). The saturation state of these fluids with respect to dypingite was not calculated owing to lack of relevant thermodynamic data. A summary of these saturation state calculations is provided in Table 2. The evolution of the saturation state of the fluids of experiments Bio-A and Abio-A are illustrated as a function of time in Fig. 5. The calculated aqueous speciation of Mg is reported in Table ESM-2 (file ESM.pdf). The aqueous speciation of Mg during the experiments was dominated by aqueous Mg^{2+}, but also contained 30–50% of $MgCO_3^{-}{}_{(aq)}$ and minor quantities of $MgHCO_3^{\circ}$ and $MgOH^{+}$.

Apparent precipitation rates (r_i) were calculated from the first derivative of the fluid phase Mg concentration with respect to time, from the onset of precipitation to the attainment of constant fluid Mg concentrations using

$$r_i = \frac{1}{\nu_{Mg,i}} \frac{dc_{Mg}}{dt} \quad (4)$$

where c_{Mg} stands for the concentration of Mg in the reactive fluid, t designates time, and $\nu_{Mg,i}$ denotes the number of moles of Mg in one mole of the i^{th} mineral. Resulting precipitation rates are presented in Table 2. All experiments performed in the presence of sterile humid air bubbling attained steady-state Mg concentrations over shorter time periods (12 ± 3 days) and exhibit higher apparent precipitation rates compared to bubbling-free experiments. Note that the Mg concentration in all the biotic experiments attained a lower stationary-state compared to those of the abiotic experiments. There is, however, no statistical difference in the precipitation rates obtained from the biotic (Bio-A and Bio-B) and abiotic (Abio-A, Abio-B, Abio-D1, Abio-D2, and Abio-E) experiments performed with either stirring or air bubbling during first 10–15 days with rates equal to $-143 \pm 33 \times 10^{-3}$ and $-118 \pm 16 \times 10^{-3}$ mol dypingite L^{-1} day^{-1}, respectively as calculated using Eq. (4).

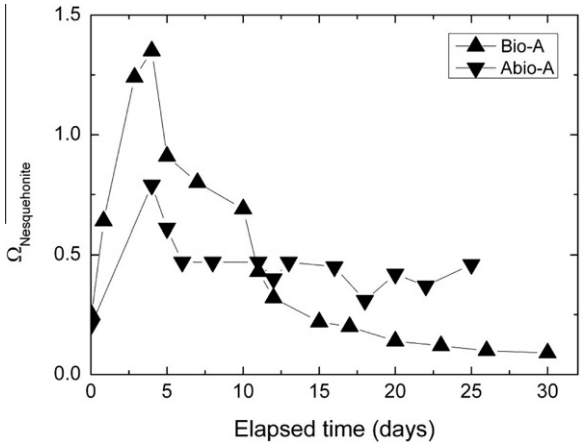

Fig. 5. Temporal evolution of saturation index of nesquehonite ($\Omega_{nesquehonite}$) of the reactive fluids during experiments Bio-A and Abio-A.

3.3. Magnesium isotopic composition

The Mg isotope compositions of all analyzed samples are given in Table 3. Mg isotope analyses were performed on selected samples of experiments Bio-A, Bio-B, Bio-C,

Table 2
Ionic Activity Product (IAP) and degree of saturation with respect to hydromagnesite and nesquehonite of the fluid at its final steady-state condition of each experiment and apparent precipitation rates for biotic and abiotic experiments. Rates are reported in moles of precipitated mineral per liter per day. Uncertainty in precipitation rates is estimated to be 10–15%.

Experiment	$IAP_{Hydromagnesite}$	$IAP_{Nesquehonite}$	Number of values used for the average	$\Omega_{Hydromagnesite}$	$\Omega_{Nesquehonite}$	dc_{Mg}/dt (10^{-3} mol Mg L^{-1} day^{-1})	Elapsed time (days)	Mineralogy
Bio-A	1.2E-34	9.0E-07	4	0.01	0.11	−1.81	15	Dypingite
Bio-B	2.2E-32	5.6E-06	4	1.71	0.69	−1.13	11	Nesquehonite
Bio-C	9.0E-34	2.9E-06	4	0.07	0.36	−0.68	40	Dypingite
Bio-D	5.3E-34	2.7E-06	4	0.04	0.33	−0.55	40	Dypingite
Bio-E	3.2E-33	6.0E-06	4	0.26	0.74	−0.38	34	Dypingite + Nesquehonite
Bio-F	1.0E-32	6.8E-06	4	0.82	0.84	−0.26	45	Nesquehonite
Bio-G	5.5E-33	3.5E-06	4	0.43	0.43	−0.31	40	Nesquehonite
Bio-I	6.1E-33	6.0E-06	4	0.48	0.75	−0.19	74	Nesquehonite
Abio-A	1.7E-34	3.2E-06	4	0.01	0.39	−1.23	12	Dypingite
Abio-B	4.8E-33	6.7E-06	4	0.38	0.83	−1.58	14	Nesquehonite
Abio-C	3.0E-33	6.6E-06	4	0.24	0.82	−0.75	15	Nesquehonite
Abio-D1	6.7E-33	7.1E-06	4	0.53	0.87	−0.95	10	Nesquehonite
Abio-D2	9.9E-35	3.1E-06	5	0.01	0.38	−1.06	12	Dypingite
Abio-E	4.6E-33	6.7E-06	4	0.36	0.83	−1.21	11	Nesquehonite

Table 3
Magnesium isotopic composition of liquid and solid samples, and fractionation factors, $\Delta^{25}Mg_{solid-liquid}$ and $\Delta^{26}Mg_{solid-liquid}$ in selected samples. Uncertainty is <0.07‰ for all measurements according to the standard deviation of replicate standards.

Sample	Mg fraction in solution	Liquid samples				Solid samples				$\Delta^{25}Mg_{solid-liquid}$	$\Delta^{26}Mg_{solid-liquid}$	Mineralogy[a]
		$\delta^{25}Mg$ (‰)	2σ	$\delta^{26}Mg$ (‰)	2σ	$\delta^{25}Mg$ (‰)	2σ	$\delta^{26}Mg$ (‰)	2σ			
Bio-A-1	0.98	−0.25	0.03	−0.52	0.05	−0.57	0.04	−1.15	0.05	−0.31	−0.63	N
Bio-A-3	0.97	−0.29	0.03	−0.55	0.03							
Bio-A-4	0.87					−0.38	0.01	−0.76	0.02			D
Bio-A-5	0.74	−0.01	0.02	−0.02	0.01							
Bio-A-7	0.57	0.04	0.03	0.07	0.04							
Bio-A-9	0.46	0.1	0.03	0.2	0.04	−0.59	0.01	−1.14	0.04	−0.69	−1.33	D
Bio-A-10	0.22	0.3	0.01	0.6	0.02							
Bio-A-12	0.16	0.36	0.03	0.71	0.06					−0.80	-1.55	
Bio-A-13	0.17	0.36	0.03	0.69	0.03	−0.44	0.01	−0.84	0.03			D
Bio-A-14	0.16	0.26	0.05	0.51	0.07							
Bio-A-15	0.13	0.06	0.01	0.13	0.01	−0.56	0.01	−1.07	0.01	−0.62	−1.21	D
Bio-B-1	1	−0.36	0.04	−0.69	0.02							
Bio-B-5	0.65	−0.25	0.06	−0.43	0.04							
Bio-B-11	0.49	−0.07	0.01	−0.13	0.03	−0.68	0.03	−1.33	0.05	−0.61	−1.19	D
Bio-C-1	1	−0.27	0.03	−0.52	0.01							
Bio-C-5	0.21	0.22	0.02	0.42	0.02	−0.54	0.03	−1.05	0.03	−0.76	−1.47	D
Bio-D-1	1	−0.34	0.02	−0.66	0.01							
Bio-D-3	0.26	0.18	0.02	0.33	0.02	−0.46	0.02	−0.9	0.02	−0.63	−1.23	D
Abio-A-1	1	−0.32	0.02	−0.62	0.05							
Abio-A-2	0.62	−0.23	0.02	−0.45	0.01							
Abio-A-5	0.47	−0.05	0.01	−0.11	0.01	−0.67	0.01	−1.28	0.03	−0.61	−1.17	D
Abio-A-10	0.34	−0.01	0.01	0.01	0.02	−0.64	0.02	−1.21	0.03	−0.64	−1.22	D
Abio-A-13	0.44	0.19	0.03	0.37	0.05	−0.56	0.03	−1.06	0.04	−0.75	−1.43	D
$MgCl_2$ (initial solution)		−0.27	0.02	−0.53	0.02							
$MgSO_4$ (BG-11)		−0.47	0.03	−0.91	0.01							
Min-free: cells after 11 days	0.9					−0.36	0.03	−0.71	0.02	0.11[b]	0.18[b]	
Min-free: cells after 44 days	0.9					−0.46	0.02	−0.87	0.02	0.01[b]	0.04[b]	

[a] Where N and D stands for nesquehonite and dypingite.
[b] $\Delta^{x}Mg$ values for Min-free experiment samples denote fractionation between initial $MgSO_4$ and the sample.

Bio-D, and Abio-A where dypingite was the main precipitated mineral phase. Furthermore, the temporal evolution of $\delta^{26}Mg$ during experiments Bio-A and Abio-A was studied in detail and is plotted in Fig. 6.

All experiments exhibited mass-dependent fractionation between fluid and solid phases. The precipitated solids have $\delta^{26}Mg$ values that are 0.63–1.55‰ lighter than their liquid counterparts. The solid samples obtained from Bio-A do not exhibit a systematic temporal trend, whilst the solid phases from the Abio-A experiment show a slight isotopic enrichment with time, concurrent with a corresponding enrichment in the reactive fluid from the same experiment. Isotopic compositions from the mineral-free experiment (Min-free) show that the *Gloeocapsa* sp. cells have slightly heavier Mg isotopic composition compared to the growth medium. The observed shift of $\delta^{26}Mg$ between the biomass and the nutrient media over the 44 days of growth during experiment Min-free is ~0.2‰.

The fractionation factors, $\Delta^{25}Mg_{solid-liquid}$ and $\Delta^{26}Mg_{solid-liquid}$, calculated from corresponding solid and liquid samples are listed in Table 3. In the presence of *Gloeocapsa* sp., $\Delta^{26}Mg_{solid-liquid}$ calculated from the first collected sample (~ after 4 h) of experiment Bio-A is significantly lower than that of the latter samples; this is the only Mg isotope concentration measurement made on nesquehonite in this study. The samples collected between 8 and 25 days from the Abio-A control experiment exhibit $\Delta^{26}Mg_{solid-liquid}$ values similar to those measured in most of the biotic experiments. There is no statistically significant correlation between the degree of Mg fractionation and the reactive fluid pH, the ion activity product of hydromagnesite ($IAP_{hydromagnesite}$), Mg concentration, alkalinity, and biomass concentrations as illustrated in Fig. ESM-1. In addition, no statistically significant correlation was found between the Mg fractionation factor and the aqueous speciation of Mg as shown in Fig. ESM-2 for $MgCO_3°(aq)$.

The temporal $\delta^{26}Mg_{solid-liquid}$ evolution of experiments Bio-A and Abio-A are plotted against fraction of Mg remaining in solution in Fig. 7. Most data from these experiments fall on parallel linear trends corresponding to constant $\Delta^{26}Mg_{solid-solution}$ and consistent with closed system equilibrium exchange between the fluid and solid phase calculated with Eq. (4).

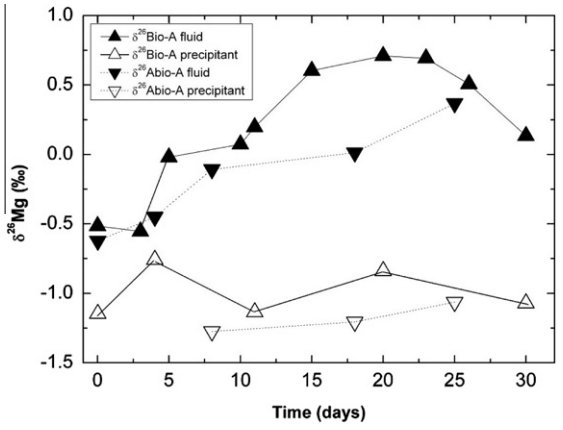

Fig. 6. Temporal evolution of $\delta^{26}Mg$ in the fluid and solid samples collected during experiments Bio-A and Abio-A. Size of the symbols incorporates the uncertainty (2σ) on the measured $\delta^{26}Mg$ values.

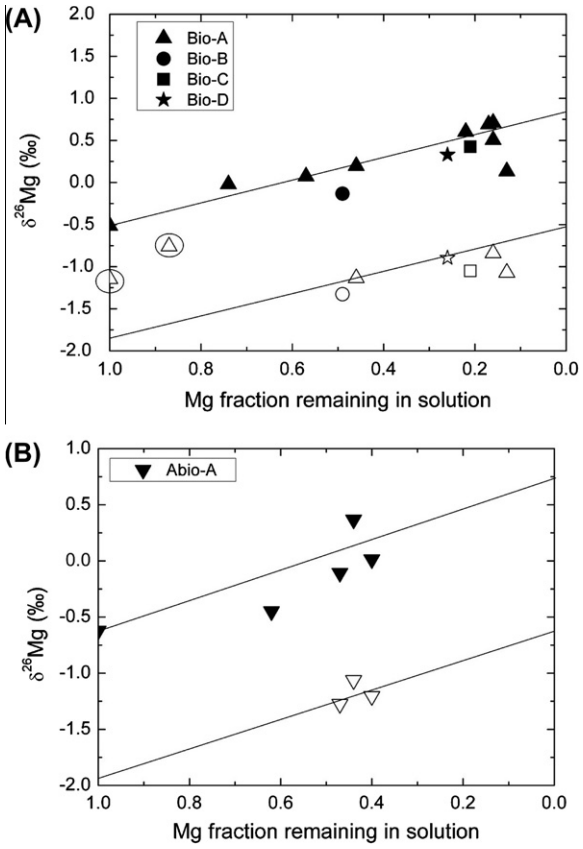

Fig. 7. $\delta^{26}Mg$ values vs. Mg fraction remaining in solution for (A) biotic experiments Bio-A, Bio-B, Bio-C, Bio-D, and (B) abiotic experiment Abio-A. The solid lines in the figure correspond to trends predicted for closed system equilibrium using Eq. (3) together with the mean measured $\Delta^{26}_{solid-liquid}$ value (-1.31 ± 0.14‰) and the $\delta^{26}Mg$ value of the $MgCl_2$ used to create the reactive fluids. Closed and open symbols correspond to liquid and solid samples, respectively. Encircled symbols collected at the beginning of experiment Bio-A which may be affected by mineralogical changes or kinetic isotopic fractionation.

4. DISCUSSION

4.1. Chemical composition of reactive fluids and precipitant mineralogy

pH was observed to increase with time in all abiotic and biotic experiments. In the abiotic experiments, this increase originates from the degassing of the initial reactive fluid, which contained a 5×10^{-2} mol/kg $NaHCO_3$ at pH ~8.5. Owing to this high aqueous bicarbonate content, these initial fluids have a pCO_2 of $10^{-2.0}$ atm, which is supersaturated with respect to the atmosphere. The bubbling of sterile humid air liberates CO_2 from the reactive fluid leading to both an increase in pH and degree of reactive fluid supersaturation with respect to Mg carbonate minerals. In

biotic experiments, this pCO_2 decrease was accompanied with an additional pH increase due to the photosynthetic uptake of HCO_3^- ions and OH^- release. This enhanced pH increase is evident in our experiments; the pH in our biotic experiments increases by 0.8–2.2 units compared to a 0.7–1.4 units increase in our abiotic experiments. Similar pH increases due to biological activity were documented by Power et al. (2007) who performed field experiments using a consortium of cyanobacteria isolated from microbial mats of hydromagnesite playas in British Columbia, Canada. The evolution of fluid composition during our experiments, as illustrated in Fig. 4, shows that, in the presence of cyanobacteria, there is initial induction period lasting up to 5 days, during which little mineral precipitation occurs. At the end of this induction period, hydroxyl ions produced by photosynthetic activity increase pH and the degree of fluid supersaturation with respect to hydrous magnesium carbonates leading to their precipitation (see also Thompson and Ferris, 1990). Indeed, the TEM images shown in Fig. 3, and the corresponding EDX analyses, of active *Gloeocapsa* sp. cyanobacteria suspension in fluids supersaturated with respect to magnesium carbonates show the formation of a fine grained mineral phase in the near their surfaces, indicating a strong link between cyanobacterial cells and the precipitating Mg carbonate.

The final mineral phase precipitated in our experiments was either dypingite, a rare hydrous magnesium carbonate mineral compositionally similar to hydromagnesite (Raade, 1970) or nesquehonite. Note that all experiments were oversaturated with respect to hydromagnesite, although this mineral phase was not observed to precipitate. Power et al. (2007) reported dypingite formation in biotic mesocosm experiments, and nesquehonite formation in abiotic control experiments at a pH of ~9.5. The transformation of nesquehonite to hydromagnesite is known to occur through intermediary hydrous magnesium carbonate phases such as dypingite (Davies and Bubela, 1973; Hopkinson et al., 2008). Although it has been argued that such mineralogical changes could be an artifact of the sample drying (Botha and Strydom, 2001), we did not observe any significant difference in the XRD patterns of samples prepared via freeze-drying and those oven-drying at 50 °C, and thus conclude that mineralogical changes did not occur during sample preparation. All previous reported work on the transformation of nesquehonite to hydromagnesite was performed at temperatures above 45 °C, suggesting that this is an optimum temperature for this reaction. Formation of hydromagnesite, however, in natural environments (e.g. Lake Salda, Turkey; British Columbia, Canada) likely occurs at significantly lower temperatures, similar to those of our experiments (Braithwaite and Zedef, 1994; Power et al., 2007, 2009). The results above suggest that, at ambient temperatures, the transformation from nesquehonite to hydromagnesite occurs via a dypingite intermediary both in the laboratory and in nature. However the physicochemical factors controlling these transformation reactions are currently unknown. Note that a slow transition from dypingite to hydromagnesite, might explain the differences reported above between our XRD spectra and the reference standard.

4.2. Role of cyanobacteria in Mg concentration and isotopic fractionation

Bacterial cell surfaces, chlorophyll-*a*, and cellular cytoplasm are strong adsorbers of aqueous ions (Pokrovsky and Savenko, 1995b; Pokrovsky and Kompantseva, 2007); as such some Mg could have absorbed to cell walls in our experiments. For example, Jasper and Silver (1977) reported that Mg can be incorporated into chlorophyll-*a* and cellular cytoplasm during cyanobacterial growth. Black et al. (2006) reported that chlorophyll-*a* isolated from cyanobacterium *Synechococcus elongatus* preferentially incorporates light Mg isotopes. This process has also been observed to enrich cells in heavy Zn isotopes (Gélabert et al., 2006). The maximum surface site density of *Gloeocapsa* sp., as revealed by proton Ca–Mg exchange experiments, is $\sim 0.7 \times 10^{-3}$ mol g_{dry}^{-1} (Pokrovsky et al., 2008). This suggests that the maximum amount of Mg removed from the reactive fluid during our experiments performed in the presence of cyanobacteria, which contained 2–3 g_{dry} biomass L^{-1} is no more than 1.4–2.1 $\times 10^{-3}$ mol L^{-1}. This is significantly smaller than the 15–25 $\times 10^{-3}$ mol L^{-1} of Mg removed from solution by mineral precipitation in our experiments. The small role of bacterial adsorption in this study is confirmed by the results of experiment Min-free. This experiment, performed to quantify Mg uptake and fractionation by *Gloeocapsa* sp. shows that only 1.5×10^{-5} to 2.5×10^{-5} mol L^{-1} of the aqueous Mg concentration in the reactive fluid was taken up by the biomass. Therefore, unless the isotopic fractionation linked to Mg adsorption at cyanobacteria surface is orders of magnitude larger than suggested by previous studies, Mg adsorption on the cell surface should be negligible compared to the effects of mineral precipitation.

Note that the magnesium isotope compositions of the solid samples retrieved after 1 h and 4 days of Bio-A experiment deviate from the closed system fractionation trend shown in Fig. 7a. The observed differences between solid and fluid phases may reflect the change in the mineralogy from the initially precipitated nesquehonite to the more stable dypingite, if each mineral has a distinct fractionation factor. Another possibility is that precipitation rates are fast at the onset of the experiment, so this deviation may stem from kinetic isotopic fraction effects.

4.3. Magnesium isotope fractionation between minerals and reactive fluid

The reactive fluids of experiments Bio-A, Bio-B, Bio-C, Bio-D, and Abio-A exhibit an increase in δ^{26}Mg values of 0.5–1.5‰ (see Table 3 and Fig. 6). This demonstrates that lighter Mg isotopes are preferentially incorporated into the solid phase. This observation is coherent with the results of previous studies on Mg isotope fractionation between aqueous fluids and biogenic skeletal carbonates (Chang et al., 2004; Buhl et al., 2007; Hippler et al., 2009; Wombacher et al., 2011), abiotically precipitated low Mg-calcite (Galy et al., 2002; Immenhauser et al., 2010), dolomite (Higgins and Schrag, 2010; Pokrovsky et al., 2011), and magnesite (Pearce et al., 2009; Mavromatis et al., 2011). The origin of the Mg isotope fractionation likely stems from the change

in Mg coordination, symmetry, and bond distances in the reaction forming the mineral from the aqueous fluid. One of the main changes during this reaction is the loss of the strongly attached hydration shell surrounding Mg, which has six water molecules located at a distance of 2.08 Å (Di Tommaso and de Leeuw, 2010). In contrast, Mg in hydrous Mg carbonate minerals is contained in a three-dimensional framework of MgO_6 octahedra and triangular carbonate ions. For example, the average Mg–O distances in hydromagnesite are 2.10 and 2.04 Å where the Mg(1) atom is surrounded by four oxygen atoms from carbonate ions, one from a hydroxyl group and one from a water molecule, while the Mg(2) atom is surrounded by four oxygen atoms from carbonate groups and two from hydroxyl groups (Akao et al., 1974). As such, the Mg–O octahedra in hydromagnesite are more distorted than that in the aqueous solution. Quantum mechanic theory suggests that heavier isotopes will concentrate in the species in which they are most strongly bounded (i.e. the aqueous fluid), meaning the lighter, less stable isotopes will be favored in the solid phase (Criss, 1999). In contrast, (Li et al., 2011) reported that epsomite preferentially incorporates heavy Mg from aqueous solution. These authors attribute this contrasting behavior to the difference in strength and configuration of bonds in sulfate versus carbonate minerals.

The $\Delta^{26}Mg_{solid-liquid}$ values of abiotic experiments range from $-1.43‰$ to $-1.17‰$. These factors are similar to those found in the experiments performed in the presence of *Gloeocapsa* sp., which range from $-1.55‰$ to $-1.19‰$. Measured $\Delta^{26}Mg_{solid-liquid}$ values are consistent with a closed system equilibrium model (see Fig. 7) suggesting a continuous isotopic exchange/equilibration between the precipitated hydrous Mg-carbonates and the reactive fluid, probably via a dissolution/re-precipitation process, which itself is consistent with the equilibrium fraction model (Criss, 1999). Such a process can also explain the small temporal variations in $\Delta^{26}Mg_{solid-liquid}$ values observed during the experiments.

The observation that $\Delta^{26}Mg_{solid-liquid}$ values are identical, within uncertainty (defined as the standard deviation of all samples where solid and liquid phase were measured and is equal to $\pm 0.14‰$), in the presence and the absence of *Gloeocapsa* sp. suggests that Mg carbonate sediments formed via abiotic processes or provoked by cyanobacterial photosynthesis will exhibit similar Mg isotopic signatures. Moreover no affect of reactor stirring or air bubbling was found on Mg isotope fractionation. This suggests that the experimental fractionation factors determined in this study may be applicable to natural processes exhibiting highly variable hydrodynamic conditions and gas/fluid exchange intensity. This conclusion is supported by observations at Salda Lake (Shirokova et al., 2011); Mg fractionation between lake water and hydromagnesite at Salda Lake is equal to that measured in this experimental study. The only exception to this might be Mg-carbonate formation in biofilms that exhibit a high cell:mineral ratio, as cyanobacteria can store Ca^{2+} and Mg^{2+} ions in organic envelopes (Braissant et al., 2003, 2007). In such systems, "organic" Mg originated from cell decay and lysis would be isotopically lighter than the bulk fluid phase. Given that the $\Delta^{26}Mg_{solid-liquid}$ value for cell biomass is significantly less negative than that for inorganic carbonates, the release of Mg from cyanobacterial sheaths and cell envelopes, and subsequent precipitation of Mg carbonates in the vicinity of the cyanobacterial mats, might produce minerals that are isotopically heavier than those precipitated directly from supersaturated aqueous fluids at having a high fluid to cell biomass ratio.

Because no affect of the presence of cyanobacteria was observed in this study on Mg fractionation between the reactive fluid and precipitated hydrous magnesium carbonates one might be tempted to generalize this observation to other alkaline Earth metals (e.g. Ca, and Sr) and other carbonate minerals. Such generalizations, however, are not possible to validate or refute at present due to lack of controlled experimental data. Nevertheless, recent studies demonstrate that the presence of aqueous organic ligands such as citrate and oxalate, alter significantly the Mg isotopic fractionation between magnesite and the fluid phase (Mavromatis et al., 2011). This demonstrates that bacterial activity could alter divalent metal fractionation in minerals if they produce sufficient concentration of metal complexing aqueous organic ligands.

5. CONCLUSIONS

The hydrous magnesium carbonates nesquehonite and dypingite, were precipitated in the presence and absence of the cyanobacteria *Gloeocapsa* sp. under varying laboratory conditions (i.e. stirring and bubbling, continuous light, darkness, day/night cycle). All experiments yielded similar bulk precipitation rates, although the pH of the reactive fluids was 0.5–1.0 units higher in biotic experiments compared to abiotic experiments. Similarly, retrieved $\Delta^{26}Mg_{solid-liquid}$ values obtained from abiotic experiments are identical within uncertainty of those obtained in the presence of *Gloeocapsa* sp. Taken together these observations indicates that the presence of cyanobacteria affects neither the rates nor the Mg isotopic fractionation of the precipitated hydrous magnesium carbonates in natural systems. This conclusion suggests the Mg isotopic composition of magnesium carbonate may not be indicative of either the role of bacteria or the fluid composition of past ecosystems.

ACKNOWLEDGMENTS

The authors thank E.I. Kompantseva for providing the *Gloeocapsa* sp. culture. Remi Meyer and Jerome Chmeleff are acknowledged for their assistance with the MC–ICP-MS analyses in Toulouse and Manuela Fehr is acknowledged for her assistance with MC–ICP-MS analyses at the Open University. Adrian Immenhauser and four anonymous reviewers are thanked for their helpful comments. This work was supported by MC ITN DELTA-MIN (ITN-2008-215360), MC RTN GRASP-CO_2 (MRTN-CT-2006-035868) and MC MIN-GRO (MRTN-CT-2006-035488) and the programs: INTERVIE (INSU), EPOV (CNRS), and the Associated European Laboratory LEAGE.

APPENDIX A. SUPPLEMENTARY DATA

Supplementary data associated with this article can be found, in the online version, at doi:10.1016/j.gca.2011. 10.019.

REFERENCES

Akao M., Marumo F. and Iwai S. (1974) The crystal structure of hydromagnesite. *Acta Cryst.* **B30**, 2670.

Altermann W., Kazmierczak J., Oren A. and Wright D. T. (2006) Cyanobacterial calcification and its rock-building potential during 3.5 billion years of Earth history. *Geobiology* **4**, 147–166.

Black J. R., Yin Q. Z. and Casey W. H. (2006) An experimental study of magnesium-isotope fractionation in chlorophyll-a photosynthesis. *Geochim. Cosmochim. Acta* **70**, 4072–4079.

Botha A. and Strydom C. A. (2001) Preparation of a magnesium hydroxy carbonate from magnesium hydroxide. *Hydrometallurgy* **62**, 175–183.

Brady A. L., Slater G., Laval B. and Lim D. S. (2009) Constraining carbon sources and growth rates of freshwater microbialites in Pavilion Lake using ^{14}C analysis. *Geobiology* **7**, 544–555.

Braissant O., Cailleau G., Dupraz C. and Verrecchia A. P. (2003) Bacterially induced mineralization of calcium carbonate in terrestrial environments: the role of exopolysaccharides and amino acids. *J. Sediment. Res.* **73**, 485–490.

Braissant O., Decho A. W., Dupraz C., Glunk C., Przekop K. M. and Visscher P. T. (2007) Exopolymeric substances of sulfate-reducing bacteria: interactions with calcium at alkaline pH and implication for formation of carbonate minerals. *Geobiology* **5**, 401–411.

Braithwaite C. J. R. and Zedef V. (1994) Living hydromagnesite stromatolites from Turkey. *Sediment. Geol.* **92**, 1–5.

Buhl D., Immenhauser A., Smeulders G., Kabiri L. and Richter D. K. (2007) Time series $\delta^{26}Mg$ analysis in speleothem calcite: kinetic versus equilibrium fractionation, comparison with other proxies and implications for palaeoclimate research. *Chem. Geol.* **244**, 715–729.

Chafetz H. S. and Buczynski C. (1992) Bacterially induced lithification of microbial mats. *Palaios* **7**, 277–293.

Cheng W. T. and Li Z. B. (2010a) Controlled supersaturation precipitation of hydromagnesite for the $MgCl_2$–Na_2CO_3 system at elevated temperatures: chemical modeling and experiment. *Ind. Eng. Chem. Res.* **49**, 1964–1974.

Cheng W. T. and Li Z. B. (2010b) Nucleation kinetics of nesquehonite ($MgCO_3$ $3H_2O$) in the $MgCl_2$–Na_2CO_3 system. *J. Cryst. Growth* **312**, 1563–1571.

Chang V. T. C., Makishima A., Belshaw N. S. and O'Nions R. K. (2003) Purification of Mg from low-Mg biogenic carbonates for isotope ratio determination using multiple collector ICP-MS. *J. Anal. At. Spectrom.* **18**, 296–301.

Chang V. T. C., Williams R. J. P., Makishima A., Belshawl N. S. and O'Nions R. K. (2004) Mg and Ca isotope fractionation during $CaCO_3$ biomineralisation. *Biochem. Biophys. Res. Commun.* **323**, 79–85.

Criss R. E. (1999) *Principles of Stable Isotope Distribution*. Oxford University Press, Oxford.

Davies P. J. and Bubela B. (1973) Transformation of nesquehonite into hydromagnesite. *Chem. Geol.* **12**, 289–300.

Di Tommaso D. and de Leeuw N. H. (2010) Structure and dynamics of the hydrated magnesium ion and of the solvated magnesium carbonates: insights from first principles simulations. *Phys. Chem. Chem. Phys.* **12**, 894–901.

Douglas S. and Beveridge T. J. (1998) Mineral formation by bacteria in natural microbial communities. *FEMS Microbiol. Ecol.* **26**, 79–88.

Dove P. M. (2010) The rise of skeletal biominerals. *Elements* **6**, 37–42.

Dupraz C., Reid R. P., Braissant O., Decho A. W., Norman R. S. and Visscher P. T. (2009) Processes of carbonate precipitation in modern microbial mats. *Earth-Sci. Rev.* **96**, 141–162.

Ferris F. G., Thompson J. B. and Beveridge T. J. (1997) Modern freshwater microbialites from Kelly Lake, British Columbia, Canada. *Palaios* **12**, 213–219.

Galy A., Belshaw N. S., Halicz L. and O'Nions R. K. (2001) High-precision measurement of magnesium isotopes by multiple-collector inductively coupled plasma mass spectrometry. *Int. J. Mass Spectrom.* **208**, 89–98.

Galy A., Bar-Mattews M., Halicz L. and O'Nions R. K. (2002) Mg isotopic composition of carbonate: insight from speleotherm formation. *Earth Planet. Sci. Lett.* **201**, 105–115.

Gélabert A., Pokrovsky O. S., Viers J., Schott J., Boudou A. and Feurtet-Mazel A. (2006) Interaction between zinc and freshwater and marine diatom species: surface complexation and Zn isotope fractionation. *Geochim. Cosmochim. Acta* **70**, 839–857.

Goldstein S. L., Deines P., Oelkers E. H., Rudnik R. L. and Walter L. M. (2003) Standards for publication of isotopic ratio and chemical data in chemical geology. *Chem. Geol.* **202**, 1–4.

Higgins J. A. and Schrag D. P. (2010) Constraining magnesium cycling in marine sediments using magnesium isotopes. *Geochim. Cosmochim. Acta* **74**, 5039–5053.

Hippler D., Buhl D., Witbaard R., Richter D. K. and Immenhauser A. (2009) Towards a better understanding of magnesium-isotope ratios from marine skeletal carbonates. *Geochim. Cosmochim. Acta* **73**, 6134–6146.

Hopkinson L., Rutt K. and Cressey G. (2008) The transformation of nesquehonite to hydromagnesite in the system CaO–MgO–H_2O–CO_2: an experimental spectroscopic study. *J. Geol.* **116**, 387–400.

Immenhauser A., Buhl D., Richter D., Niedermayr A., Riechelmann D., Dietzel M. and Schulte U. (2010) Magnesium-isotope fractionation during low-Mg calcite precipitation in a limestone cave – Field study and experiments. *Geochim. Cosmochim. Acta* **74**, 4346–4364.

Jasper P. and Silver S. (1977) Magnesium transport in microorganisms. In *Microorganisms and Minerals*, vol. 3 (ed. E. D. Weinberg). Marcel Dekker Inc., pp. 7–47.

Li W. Q., Beard B. L. and Johnson C. M. (2011) Exchange and fractionation of Mg isotopes between epsomite and saturated $MgSO_4$ solution. *Geochim. Cosmochim. Acta* **75**, 1814–1828.

Lowenstam H. A. and Weiner S. (1989) *On Biomineralization*. Oxford University Press, Oxford, New York.

Martinez R. E., Pokrovsky O. S., Schott J. and Oelkers E. H. (2008) Surface charge and zeta-potential of metabolically active and dead cyanobacteria. *J. Colloid Interface Sci.* **323**, 317–325.

Mavromatis V., Gautier Q., Schott J. and Oelkers E. H. (2011) Effect of aqueous organic ligands on Mg-isotope fractionation during magnesite precipitation. *Mineral Mag.* **75**, 1430.

Parkhurst D. L. and Appelo C. A. J. (1999) User's Guide to PHREEQC (Version 2) – *A Computer Program for Speciation, Batch- Reaction, One-Dimensional Transport, and Inverse Geochemical Calculations*. U.S. Geological Survey Water-Resources Investigations Report 99-4259, 310pp.

Pearce C. R., Saldi G. D., Schott J., Burton K. W. and Oelkers E. H. (2009) Experimental quantification of kinetic Mg-isotope fractionation during magnesite precipitation. *Geochim. Cosmochim. Acta* **73**(13), A1003.

Pentecost A. and Spiro B. (1990) Stable carbon and oxygen isotope composition of calcites associated with modern fresh-water cyanobacteria and algae. *Geomicrobiol. J.* **8**, 17–26.

Planavsky N., Reid R. P., Lyons T. W., Myshrall K. L. and Visscher P. T. (2009) Formation and diagenesis of modern marine calcified cyanobacteria. *Geobiology* **7**, 566–576.

Pokrovsky O. S. (1998) Precipitation of calcium and magnesium carbonates from homogeneous supersaturated solutions. *J. Cryst. Growth* **186**, 233–239.

Pokrovsky B. G., Mavromatis V. and Pokrovsky O. S. (2011) Co-variation of Mg and C isotopes in Late Precambrian carbonates of the Siberian Platform: a new tool for tracing the change in weathering regime? *Chem. Geol* **290**, 67–74.

Pokrovsky O. S. and Kompantseva E. I. (2007) Experimental physicochemical modeling of interactions between phototrophic microorganisms (anoxiphotobacteria and cyanobacteria) with trace elements in aqueous solutions. *Geochem. Int.* **45**, 302–307.

Pokrovsky O. S. and Savenko V. S. (1995a) Kinetics of calcium carbonate nucleation in seawater: the role of phosphates and hydrodynamics of the medium. *Oceanology* **35**(N5), 599–603.

Pokrovsky O. S. and Savenko V. S. (1995b) Experimental modeling of $CaCO_3$ precipitation at the conditions of photosynthesis in seawater. *Oceanology* **35**(N6), 805–810.

Pokrovsky O. S., Martinez R. E., Golubev S. V., Kompantseva E. I. and Shirokova L. S. (2008) Adsorption of metals and protons on Gloeocapsa sp cyanobacteria: a surface speciation approach. *Appl. Geochem.* **23**, 2574–2588.

Power I. M., Wilson S. A., Thom J. M., Dipple G. M., Gabites J. E. and Southam G. (2009) The hydromagnesite playas of Atlin, British Columbia, Canada: a biogeochemical model for CO_2 sequestration. *Chem. Geol.* **260**, 286–300.

Power I. M., Wilson S. A., Thom J. M., Dipple G. M. and Southam G. (2007) Biologically induced mineralization of dypingite by cyanobacteria from an alkaline wetland near Atlin, British Columbia, Canada. *Geochem. T.* **8**, 16.

Raade G. (1970) Dypingite, a new hydrous basic carbonate of magnesium, from Norway. *Am. Miner.* **55**, 1457–1465.

Raven J. A. and Giordano M. (2009) Biomineralization by photosynthetic organisms: evidence of co-evolution of the organisms and their environment? *Geobiology* **7**, 140–154.

Riding R. (2000) Microbial carbonates: the geological record of calcified bacterial-algal mats and biofilms. *Sedimentology* **47**, 179–214.

Shirokova L. S., Mavromatis V., Bundeleva I. A., Pokrovsky O. S., Bénézeth P., Pearce C., Gérard E., Balor S. and Oelkers E. H. (2011) Can Mg isotopes be used to trace cyanobacteria-mediated magnesium carbonate precipitation in alkaline lakes? *Biogeosci. Discuss.* **8**, 6473–6517.

Teng F. Z., Wadhwa M. and Helz R. T. (2007) Investigation of magnesium isotope fractionation during basalt differentiation: implications for a chondritic composition of the terrestrial mantle. *Earth Planet. Sci. Lett.* **261**, 84–92.

Thompson J. B. and Ferris F. G. (1990) Cyanobacterial precipitation of gypsum, calcite, and magnesite from natural alkaline lake water. *Geology* **18**, 995–998.

Wombacher F., Eisenhauer A., Böhm F., Gussone N., Regenberg M., Dullo W. C. and Rüggeberg A. (2011) Magnesium stable isotope fractionation in marine biogenic calcite and aragonite. *Geochim. Cosmochim. Acta* **75**, 5797–5818.

Young E. D. and Galy A. (2004) The isotope geochemistry and cosmochemistry of magnesium. *Rev. Mineral. Geochem.* **55**, 197–230.

Associate editor: Susan Glasauer